Particle-Scale Investigation of the Solid Dispersion and Residence Properties in a 3-D Spout-Fluid Bed

Shiliang Yang, Kun Luo, Jianren Fan, and Kefa Cen
State Key Laboratory of Clean Energy Utilization, Energy Department, Zhejiang University, Hangzhou 310027, P.R. China

DOI 10.1002/aic.14494
Published online May 21, 2014 in Wiley Online Library (wileyonlinelibrary.com)

Three-dimensional modeling of the gas–solid flow in a spout-fluid bed is conducted at the particle-scale level. Both the local and systematic dispersion behaviors of solid phase are initially investigated. Then, the solid circulating and resident behaviors are discussed. The results demonstrate that vigorously lateral solid dispersion appears in the spout region and the periphery of the fountain, whereas intensely vertical dispersion exists in the central region of the bed. Moreover, the inlet configuration of bed strongly affects the distribution of lateral dispersion, while its influence on the vertical one disappears in the fountain. Strong anisotropy of solid dispersion along the three directions is obtained. Systematic dispersion intensity along the vertical direction is an order of magnitude larger than the lateral one. In addition, two circulating patterns of solid phase can be identified. Solid residence time is the smallest in the spout region and the largest in the bottom corner. © 2014 American Institute of Chemical Engineers *AIChE J*, 60: 2788–2804, 2014
Keywords: spout-fluid bed, solid dispersion, particle circulation, solid residence time, discrete element method

Introduction

Spout-fluid bed is a kind of fluidizing apparatus which has been frequently applied in many physical and chemical processes, such as drying of granulation,[1] coating of the tablet,[2] and coal gasification.[3,4] As compared with the traditionally bubbling fluidized bed and conical spouted bed, the additional background gas flow in the spout-fluid bed leads to higher circulation and mixing rates of solid phase.[5] Meanwhile, due to the cross flow of additional gas flow, the total flow rate required to fluidize the particles is smaller as compared with other fluidizing bed. Besides, the wider flow rates in this type of fluidizing apparatus provide a wider operational range without slug formation.[5]

In the past decades, plenty of experimental efforts have been made to investigate many important aspects of the spout-fluid bed, such as flow characteristic and solid circulation,[6] Shannon entropy analysis of the dynamic behavior,[7] the maximum spoutable bed height,[8] particle/gas mixing behavior,[9] the effects of collision properties on the bed dynamics,[10] and so on.

With the developments of computational ability and algorithm, discrete element method (DEM) combined with computational fluid dynamics (CFD) approach[11–15] has been proven to be a powerful tool in exploring the dynamical property of the dense fluidizing apparatus. In the coupling procedure, detailed microscopic information related to the local flow structure and interactions between particles can be easily obtained, which is beneficial to the exploration of the intrinsic solid movement mechanism in the dense gas–solid flow.[16,17] This coupling approach has been successfully applied to investigate the dynamical properties of the spout-fluid bed. Link et al.[18] presented a numerical work to study the granulation process in a spout-fluidized bed with the DEM. The results indicated that the particle growth gives rise to the change of the average diameter of particle-size distribution, but not the width of the particle diameter distribution. Link et al.[19] reported a combined experimental and numerical study on the flow regimes of a spout-fluid bed under different operational conditions. Zhang et al.[20] carried out a numerical study of the particle motion and mixing in a flat-bottom spout-fluid bed with the DEM simulation. The results indicated that the spouting gas is the driving force for the formation of particle circulation roll. van Buijtenen et al.[21] conducted a research using the discrete particle model and nonintrusive measurement techniques in a pseudo two-dimensional (2-D) triple-spout fluidized bed. The results demonstrated that the presence of multiple spouts in a spout-fluidized bed highly affects the flow behavior of each spout. Thus, the internal solid movement property cannot be distinguished by solely investigating sing-spout fluidized beds. Goniva et al.[22] recently studied the effect of rolling friction on the dynamics in a spout-fluidized bed with the CFD-DEM coupling approach.

Besides these mentioned aspects investigated by the researchers, however, rare study has been performed to investigate the solid dispersion and resident properties of solid phase in the spout-fluid bed. As the operational performance is highly influenced by the dispersion and resident behaviors of solid phase in the system, the information of solid dispersion and resident properties in the spout-fluid bed is critical for the design, optimization, and scale-up of industrial apparatus. Because the solid dispersion in the dense

Correspondence concerning this article should be addressed to J. Fan at fanjr@zju.edu.cn.

gas–solid flow is adopted to evaluate the mixing rate of solid phase in the fluidizing reactor, there has been a growing interest in exploring the solid dispersion behavior in the chemical apparatus, such as the bubbling fluidized bed,[23–27] the spouted bed,[28] the 20-L explosion vessel,[29,30] the dry powder inhalers,[31] and the circulating fluidized bed.[32,33] Recently, Zhang et al.[34] conducted an experimental study to investigate the particle dispersion in a spout-fluid bed using the microwave heating and the infrared thermal imaging technique. The results reported the effect of the fluidizing gas velocity on the particle dispersion behavior in general. Unfortunately, local dispersion behaviors of solid phase in different regions of the system have not been discussed. As three regions with significantly distinct movement behaviors of solid phase exist in the spout-fluid bed, exploring the local dispersion behavior of solid phase is the prerequisite to understand the intrinsic mechanisms of solid transportation. To our knowledge, there has not been any published research focusing on the local dispersion property of solid phase in the spout-fluid bed with either numerical or experimental approach, so far.

Furthermore, solid residence time (SRT) is an important parameter strongly influencing the bed performance and product quality. Its distribution can be utilized to characterize the mixing degree and solid motion in the system. It is crucial for the design, control, and optimization of the spout-fluid bed especially in the fluid catalytic cracking and other catalytic processes as the fast reaction rate, quick catalyst deactivation, and intense heat and mass transfers require good control of the solid mixing and residence time.[35] SRT distribution can be obtained with the experimental approach, such as postprocessing on the basis of a series of consecutive images[36] and fast response particle residence time distribution technique.[35] Due to the existence of three distinct regions in the spout-fluid bed, exploring the solid circulating pattern and quantitatively evaluating the SRT distribution play critical roles in revealing the solid transportation mechanism in the system.

Therefore, the main objective of current work is to explore the dispersion and resident behaviors of solid phase in a three-dimensional (3-D) spout-fluid bed from both the macroscopic and microscopic views with the CFD-DEM coupling approach, in which gas motion is solved in the framework of CFD and solid motion is obtained at the particle-scale level. First, the simulated time-averaged velocity of solid phase and its root mean square (RMS) are compared with the experimental data in literature to validate the proposed model. Then, the distribution property of solid dispersion coefficient is investigated to obtain the local dispersion behaviors of solid phase in different regions of the system. Moreover, the systematic dispersion coefficient is used to capture the dispersion behavior of the whole system with a macroscopic view. Finally, the local and global resident behaviors of solid phase are discussed.

Mathematical Model

Gas-phase hydrodynamics

Gas motion is governed by the volume-averaged Navier–Stokes equations by introducing the voidage in each computational cell. The mass and momentum conservation equations of gas phase can be formulated as

$$\partial\left(\varepsilon_g\rho_g\right)/\partial t+\nabla\cdot\left(\varepsilon_g\rho_g\mathbf{u}_g\right)=0 \tag{1}$$

$$\partial\left(\varepsilon_g\rho_g\mathbf{u}_g\right)/\partial t+\nabla\cdot\left(\varepsilon_g\rho_g\mathbf{u}_g\mathbf{u}_g\right)=-\varepsilon_g\nabla p_g-\sum\nolimits_{i=1}^{n}\mathbf{f}_{d,i}/\Delta V+\rho_g\varepsilon_g\mathbf{g}+\nabla\cdot\left(\varepsilon_g\tau_g\right) \tag{2}$$

In the above equations, ρ_g, $\mathbf{u}_g$, and p_g are, respectively, the density, the velocity vector, and the pressure of gas phase. t is the time instant. $\mathbf{g}$ is the gravitational acceleration. τ_g is the viscos stress tensor and can be estimated as

$$\tau_g=\mu_g[(\nabla\mathbf{u}_g)+(\nabla\mathbf{u}_g)^{-1}]+(\lambda_g-\frac{2}{3}\mu_g)(\nabla\cdot\mathbf{u}_g)\mathbf{I} \tag{3}$$

where λ_g and μ_g are the bulk viscosity and shear viscosity of gas phase, respectively. $\mathbf{I}$ is a second-order metric tensor.

The voidage ε_g is estimated as

$$\varepsilon_g=1-\frac{\sum_{i=1}^{n}V_{pi,t}}{\Delta V} \tag{4}$$

where n and ΔV are the particle number in the current cell and the volume of computational cell, respectively. As a particle may cross the borders of several neighboring cells, the segmentation approach[37] of a particle divided into 48 elements is adopted in the current work to obtain a smooth voidage field. Thus, $V_{pi,t}$ is the total volume of segment elements of particle i locating in the current cell.

$\mathbf{f}_{d,i}$ is the drag force exerted on the particle i by the gas phase and can be estimated as

$$\mathbf{f}_{d,i}=\frac{V_{pi}\beta}{(1-\varepsilon_g)}\left(\mathbf{u}_g-\boldsymbol{v}_{pi}\right) \tag{5}$$

where $\boldsymbol{v}_{pi}$ is the velocity vector of particle i. β is the interphase momentum exchanging coefficient, which is estimated from the correlation proposed by Gidaspow[38] as

$$\beta=\begin{cases}\frac{3}{4}C_D\frac{\rho_g\varepsilon_g(1-\varepsilon_g)|\mathbf{u}_g-\boldsymbol{v}_p|}{d_p}\varepsilon_g^{-2.65} & \varepsilon_g\geq 0.8\\ \frac{150(1-\varepsilon_g)^2\mu_g}{\varepsilon_g d_p^2}+\frac{1.75\rho_g(1-\varepsilon_g)|\mathbf{u}_g-\boldsymbol{v}_p|}{d_p} & \varepsilon_g<0.8\end{cases} \tag{6}$$

$$C_D=\begin{cases}\frac{24}{Re_p}\left(1+0.15\mathrm{Re}_p^{0.687}\right) & Re_p<1000\\ 0.44 & Re_p\geq 1000\end{cases} \tag{7}$$

where d_p is the particle diameter. Re_p is the particle Reynolds number and can be calculated as

$$Re_p=\frac{\rho_g\varepsilon_g|\mathbf{u}_g-\boldsymbol{v}_p|d_p}{\mu_g} \tag{8}$$

Solid motion

In the current work, solid motion is solved by means of the DEM, in which the motion of each individual particle is tracked at every time instant.[39] The translational and rotational motions of a particle are governed by the Newton's second law.[31] They are formulated as

$$m_p\frac{d\boldsymbol{v}_p}{dt}=m_p\mathbf{g}+\mathbf{f}_p+\mathbf{f}_d-\sum\nolimits_{i=1}^{k}\boldsymbol{F}_{c,i} \tag{9}$$

$$I_p\frac{d\boldsymbol{\omega}_p}{dt}=\mathbf{T}_p \tag{10}$$

where m_p and I_p are the mass and the moment of inertia of particle p, respectively. ω_p and $\mathbf{T}_p$ stand for the angular

Table 1. Details of Equations Adopted to Calculate the Parameters in Soft-Sphere Contact Model

Normal stiffness coefficient $k_{n,ij}$ and tangential stiffness coefficient $k_{t,ij}$
$k_{n,ij}=\frac{4}{3}Y^*\sqrt{R^*\delta_{n,ij}}, k_{t,ij}=8G^*\sqrt{R^*\delta_{n,ij}}$
Normal damping coefficient $\gamma_{n,ij}$ and tangential damping coefficient $\gamma_{t,ij}$
$\gamma_{n,ij}=2\sqrt{\frac{5}{6}}\psi\sqrt{S_{n,ij}m^*}, \gamma_{t,ij}=2\sqrt{\frac{5}{6}}\psi\sqrt{S_{t,ij}m^*}$
in which
$S_{n,ij}=2Y^*\sqrt{R^*\delta_{n,ij}}, S_{t,ij}=8G^*\sqrt{R^*\delta_{n,ij}}, \frac{1}{Y^*}=\frac{(1-v_i^2)}{Y_i}+\frac{(1-v_j^2)}{Y_j}$
$\frac{1}{R^*}=\frac{1}{R_i}+\frac{1}{R_j}, \frac{1}{m^*}=\frac{1}{m_i}+\frac{1}{m_j}$
$\psi=\frac{\ln(e)}{\sqrt{ln^2(e)+\pi^2}}, \frac{1}{G^*}=\frac{2(2+v_i)(1-v_i)}{Y_i}-\frac{2(2+v_j)(1-v_j)}{Y_j}$

velocity and the torque exerted on the particle, respectively. $\mathbf{f}_{p,i}(=-V_{pi}\nabla p_g)$ is the pressure gradient force exerted on particle p. $\boldsymbol{F}_{c,i}$ is the contacting force of other particles or walls colliding with the current one. k is the total number of particles and walls colliding with the current particle. Due to the dense flow property, multiple collisions exist for a particle with its neighboring ones. Hence, the soft sphere contacting model proposed by Cundall and Strack[40] is adopted to mimic the contacting procedure in the current work. The collision force between particle i and particle j can be calculated as

$$\boldsymbol{F}_{c,ij}=(k_{n,ij}\delta_{n,ij}\boldsymbol{n}+\gamma_{n,ij}\boldsymbol{v}_{n,ij})+(k_{t,ij}\delta_{t,ij}\boldsymbol{t}+\gamma_{t,ij}\boldsymbol{v}_{t,ij}) \tag{11}$$

In the above equations, $\boldsymbol{n}$ and $\boldsymbol{t}$ are the normal and tangential unit vectors between a colliding pair, respectively. $\delta_{n,ij}$ and $\delta_{t,ij}$ are the relative displacements in the normal and tangential directions, respectively. The subscripts n and t stand for the normal and tangential components of a variable, respectively. $\boldsymbol{v}_{n,ij}$ and $\boldsymbol{v}_{t,ij}$ are, respectively, the normal and tangential components of the relative velocity between colliding pair. k and γ are the stiffness coefficient and the damping coefficient, respectively. The calculation details are listed in Table 1. For the contacting force calculation between the particle and wall, the wall is treated as a stagnant particle with infinite radius and mass. Then, the collision procedure is estimated as the method for the particle–particle collision.

Solid dispersion coefficient

The dispersion intensity of solid phase is quantitatively described by means of solid dispersion coefficient. There exist two distinct methods estimating the solid dispersion coefficient, namely the macro approach and the micro approach.[28] In the macro approach, solid dispersion coefficient is calculated based on the Fick's diffusion law, which indicates that solid phase in the regions with high concentration tends to diffuse to the regions with low concentration until a dynamic equilibrium of a relatively uniform state is reached. Hence, the solid dispersion coefficient can be obtained through fitting the transient solid concentration profile by a Fickian-type diffusion equation.[26] In the micro approach, the solid dispersion coefficient is evaluated based on the particle displacement in a Lagrangian view by Einstein's equations,[26] which can be formulated as

$$D_i=\frac{(\Delta r_i)^2}{2\Delta t} \tag{12}$$

where D_i is the local dispersion coefficient of particle i. Δr_i is the local displacement of current particle in the time interval of Δt.

According to the above calculation equation, all the experimental investigations of solid dispersion coefficient in each direction of gas–solid flow system are based on the statistical average of the tracers' dispersion coefficients along the trajectories.[23,41,42] With the advantage of DEM, detailed information such as the velocity and position can be easily extracted during the calculation, which brings convenience to estimate the solid dispersion coefficients in all the three directions. In the numerical work of Liu and Chen,[26] only the lateral dispersion coefficient of solid phase in a bubbling fluidized bed is calculated using the fictitious particle to follow the solid movement at the computational grid level. Then, the dispersion coefficient of solid phase is obtained by averaging the dispersion coefficients of all the tracers.

It is obvious that all the calculation approaches mentioned above exhibit only the global dynamical property of solid dispersion in the system. Due to the chaotic, unsteady, heterogeneous, and complex characteristics of dense two-phase flow system, distinct flow behavior and solid concentration exist in different regions of the bed. Hence, the current work proposes an alternative calculation approach to evaluate the local solid coefficient at the particle-scale level with the ability of CFD-DEM coupling approach.

The local dispersion coefficient of solid phase in a specific computational cell labeled l is calculated by averaging all the dispersion coefficients of particles locating in the current cell. It can be formulated as

$$\overline{D_l}=\frac{\sum_{i=1}^{n}D_{i,\mathrm{local}}}{n}=\frac{1}{n}\sum_{i=1}^{n}\left(\frac{(\Delta r_i)^2}{2\Delta t}\right)=\frac{1}{2\times\Delta t\times n}\sum_{i=1}^{n}(\Delta r_i)^2 \tag{13}$$

where n is the total number of particles in the current computational cell. $D_{i,\mathrm{local}}$ is the local instantaneous dispersion coefficient of particle i in the time interval Δt. Δr is the displacement of particle i in a specific direction. Hence, the instantaneous dispersion coefficients of solid phase in all the computational grid cells can be obtained, leading to the appearance of a field of solid dispersion coefficient. However, the instantaneous local dispersion coefficient strongly depends on the local flow structure of gas–solid phase at a given time instant, resulting in a large fluctuation due to the frequent variations of related solid properties. To overcome this issue, the time-statistical approach is applied for entire local dispersion field to capture the solid dispersion behavior in the whole calculation domain.

Meanwhile, there is a need to evaluate the dispersion behavior of whole system in a macroscopic view, based on which other related studies, such as the influences of operating parameters or particle properties on the solid dispersion can be investigated. Hence, the systematic dispersion coefficient is presented to describe the solid dispersion behavior of the whole system. It is averaged over the instantaneous dispersion coefficients of all the particles in the current system and can be expressed as

$$D=\frac{1}{N_p}\sum_{i=1}^{N_p}\frac{(\Delta r_i)^2}{2\Delta t}=\frac{1}{N_p}\sum_{i=1}^{N_p}\frac{(r_i-r_{i0})^2}{2\Delta t}(i=1,2,...,N_p) \tag{14}$$

where N_p is the total number of particles in the system. Similarly, the dispersion intensity of solid phase in a specific region of fluidizing apparatus, such as the annulus of the spout-fluid bed, can be evaluated by dispersion intensities of all the particles involved in this region.

Time-averaged mean and RMS of solid velocity

As the solid motion is resolved at the particle-scale level in the current work, the particle velocity should be mapped into the Eulerian grid to obtain its local distribution property. According to the particle position, the computational cell that this particle locates is obtained. For a specific grid, the solid velocity of this grid at time instant j is averaged over all the velocities of particles in this cell. It is formulated as

$$\mathbf{U}_{\mathrm{s}}^{j}=\frac{\sum_{i=1}^{n_j}\boldsymbol{v}_{pi}}{n_j} \tag{15}$$

where n_j is the total number of particles locating in this cell at time instant j.

Then, the time-averaged value of solid velocity is calculated over all the instantaneous velocities of solid phase over time and can be expressed as

$$\mathbf{U}_{\mathrm{s}}=\frac{\sum_{j=1}^{N_t}\mathbf{U}_{\mathrm{s}}^{j}}{N_t} \tag{16}$$

Here, N_t is the total number of samples used to average. To evaluate its velocity fluctuation property of solid phase, the RMS of solid velocity fluctuation is adopted. Its components in the x, y, and z directions are formulated as

$$\mathrm{U}'_{\mathrm{s},i}=\sqrt{\frac{\sum_{j=1}^{N_t}\left(\mathrm{U}_{\mathrm{s},i}{}^{j}-\mathrm{U}_{\mathrm{s},i}\right)^2}{N_t}},\ i=x,y,z \tag{17}$$

where $\mathrm{U}_{\mathrm{s},i}^{j}$ is the i-component of instantaneous solid velocity at time instant j. $\mathrm{U}_{\mathrm{s},i}$ is the i-component of time-averaged solid velocity.

Computational Details

Numerical schemes

The CFD-DEM coupling procedure has been well documented in the literature.[43] The governing equations of gas motion are discretized with the finite volume method based on the collocated grid. For the discretization of the governing equations, the Crank–Nicolson scheme is adopted for the time-related items in the equations; the diffusion items and convective items are discretized with the central difference scheme and first-order up-wind scheme, respectively. The Pressure Implicit with Splitting of Operator algorithm[44] is applied for the decoupling of pressure and velocity. To update the position and velocity of solid phase in the tracking procedure, the Newton's governing equations of solid motion are explicitly integrated.

Computational conditions

The simulated spout-fluid bed is exactly the same as that used in the experimental and numerical work of Link et al.[19] The experiments are conducted separately by the two groups in the University of Twente in the Netherland and the University of Birmingham in the United Kingdom,[19] respectively. As schematically illustrated in Figure 1a, it is a cubical vessel with a width, depth, and height of 0.154 m, 0.084 m, and 1.0 m, respectively. Structured grid, as shown in Figure 1b, is used to represent the whole calculation domain. To test the grid independence of the calculation results, the whole geometry is divided into 17×10×80, 19×12×90, and 21×14×100 elements, respectively.

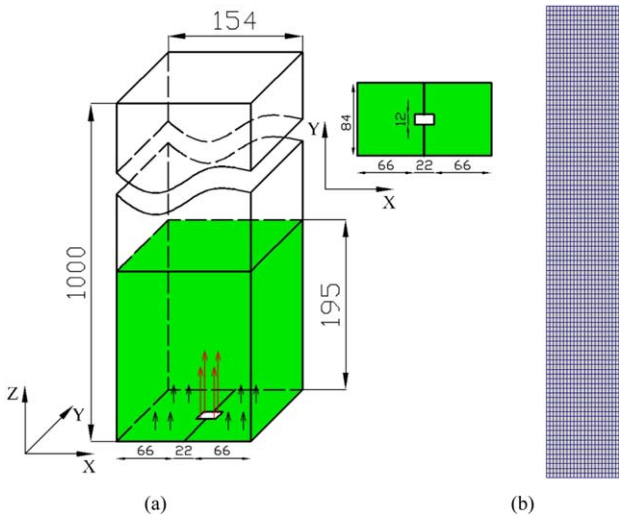

Figure 1. Sketch maps of the geometrical configuration and grid representation of computational domain (Unit: mm).

(a) 3-D view of the calculation domain; (b) front view of the computational grid (fine grid).

[Color figure can be viewed in the online issue, which is available at wileyonlinelibrary.com.]

A total number of 44,800 glass particles with diameter and density of 4.04 mm and 2526 kg/m^3, respectively, are involved in the calculation. Other material properties are adopted to be the same as those in the simulation of Link et al.[19] All the particles are generated randomly in the calculation domain and then fall down under the influence of gravity. Finally, a packed bed with a height of 0.195 m is formed above the bed inlet, from which the calculation starts. The inlet velocity of gas phase is chosen as the Case B1 in the experimental work of Link et al.,[19] namely the spout-fluid bed operates in the flow regime of spout-fluidization. Related physical and simulation parameters adopted in the current work are listed in Table 2.

To solve the governing equations of gas motion, related boundary conditions should be applied for the different

Table 2. Physical and Numerical Parameters Adopted in the Simulation

Gas phase			
Temperature, K	298	Viscosity, Pa s	1.8×10^{-5}
Spouting velocity, m/s	60	Molecular weight, kg/mol	28.8
Background velocity, m/s	2.5	Pressure, atm	1
Density, kg/m^3	1.205		
Particles (Glass)			
Number	44,800	Diameter, mm	4.04
Density, kg/m^3	2526	Young's modulus, Pa	5×10^{8}
Poisson ratio	0.2	Restitution coefficient	0.95
Friction coefficient	0.1	Dynamical rolling friction	0.05
Geometry			
Width, m	0.154	Thickness, m	0.084
Height, m	1.0		
Total number of grid cells	17×10×80 (Coarse grid resolution) 19×12×90 (Mediate grid resolution) 21×14×100 (Fine grid resolution)		

Table 3. Parameters Settings Adopted to Study the Sensitivity of Numerical Parameters to the Time-Averaged Velocity of Solid Phase

	Y_p (Pa)	v (-)	e (-)	μ_p (-)	μ_{df} (-)
Influence of Young's modulus	5×10^{10}, 5×10^{9}, 5×10^{8}, 5×10^{7}, 5×10^{6}	0.2	0.97	0.1	0.05
Influence of Poisson ratio	5×10^{8}	0.2, 0.25, 0.3	0.97	0.1	0.05
Influence of restitution coefficient	5×10^{8}	0.2	0.97, 0.95, 0.9, 0.85, 0.8	0.1	0.05
Influence of friction coefficient	5×10^{8}	0.2	0.97	0.1, 0.2, 0.25, 0.3	0.05
Influence of rolling friction	5×10^{8}	0.2	0.97	0.1	0.0, 0.05, 0.10

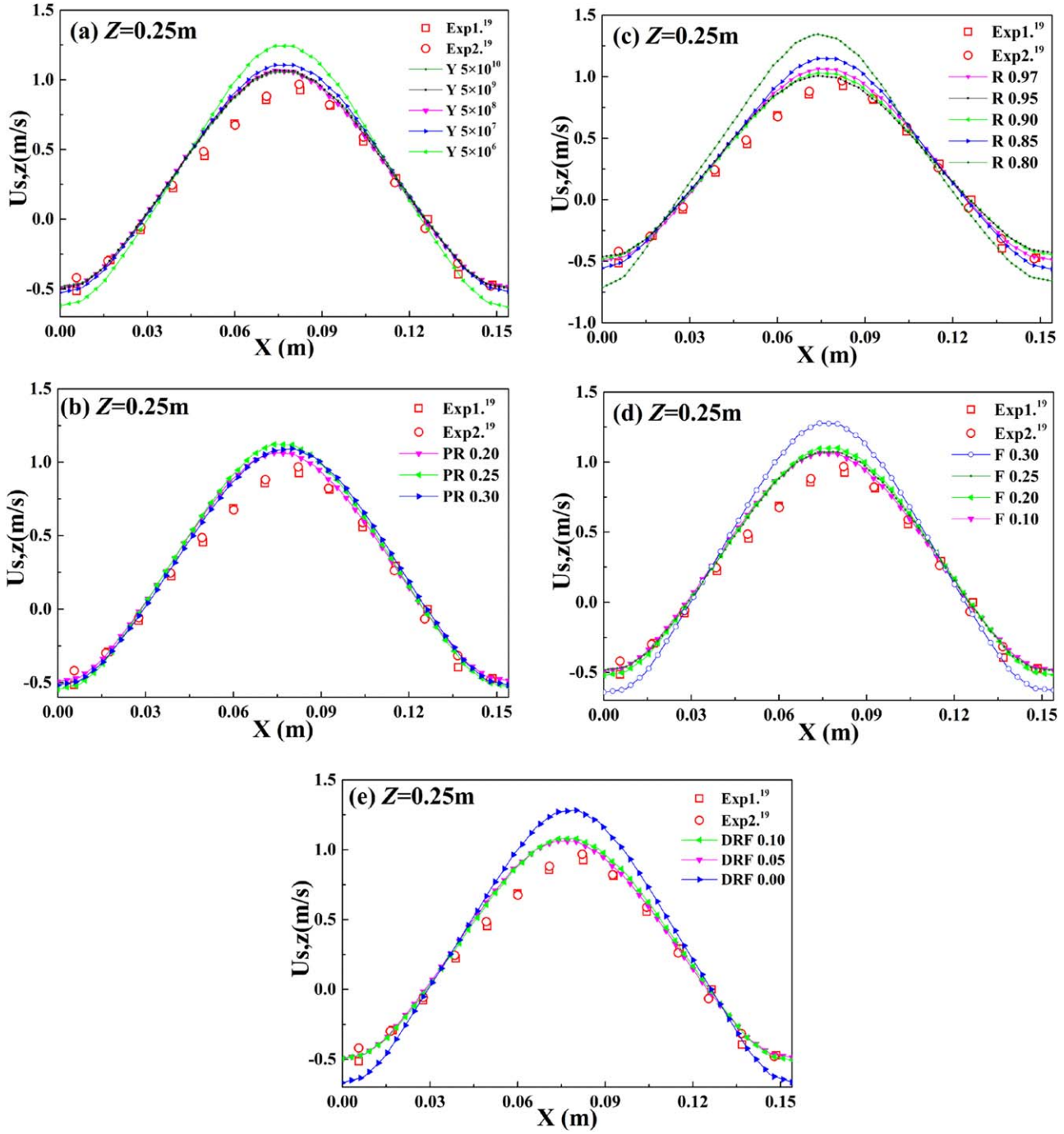

Figure 2. Sensitivity of the time-averaged vertical velocity of solid phase to the parameters settings adopted in the DEM model, $Z = 0.25$ m.

(a) Influence of Young's modulus (Y); (b) influence of Poisson ratio (PR); (c) influence of restitution coefficient (R); (d) influence of friction coefficient (F); (e) influence of dynamical rolling friction (DRF).

[Color figure can be viewed in the online issue, which is available at wileyonlinelibrary.com.]

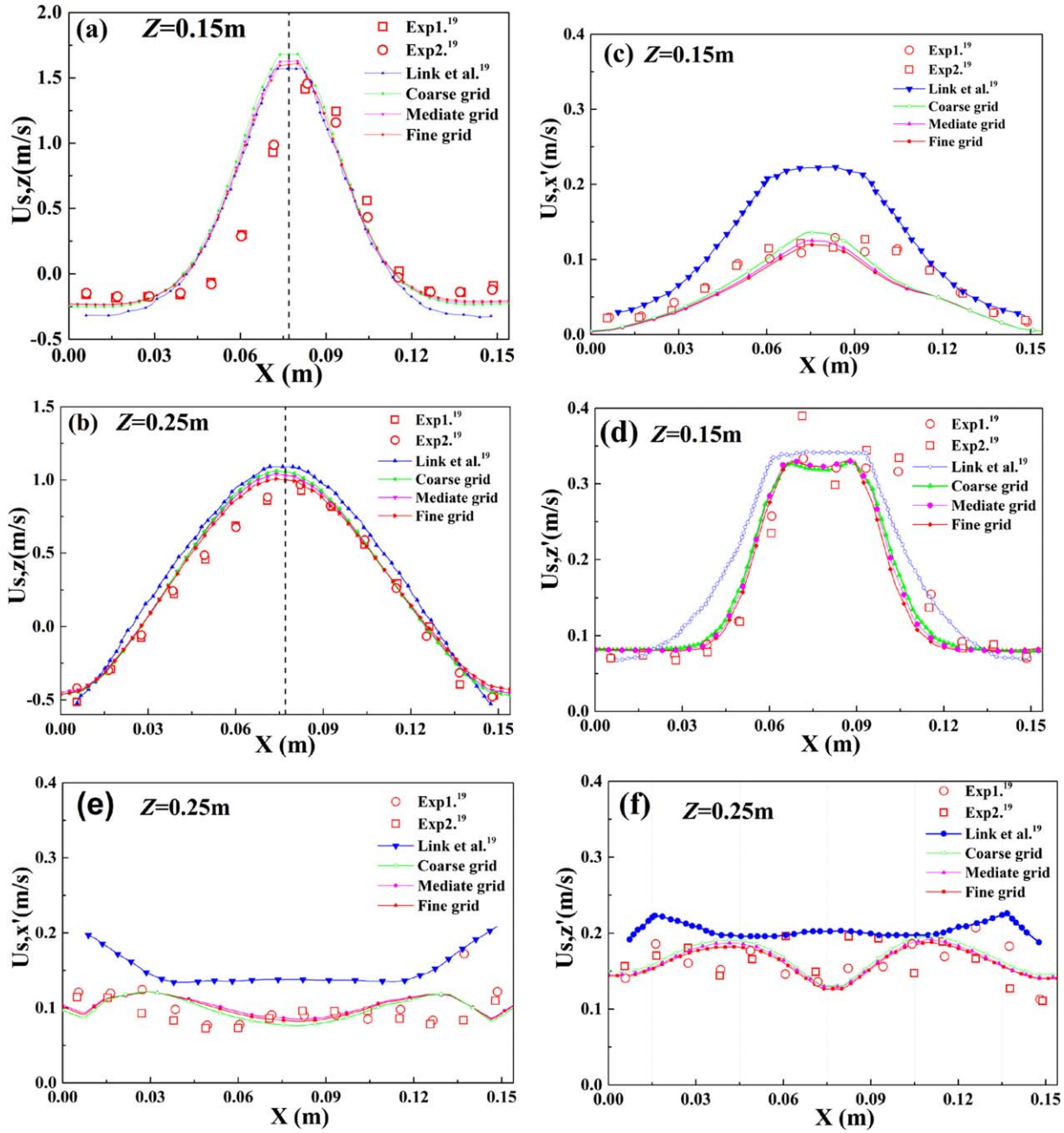

Figure 3. Comparisons of the time-averaged properties of solid phase with the experimental data[19] and the simulation of Link et al.[19] at two different heights of slice $Y = 0.042$ m (Exp1. and Exp2. stand for the experimental data obtained separately at the University of Twente in the Netherlands and the University of Birmingham in the United Kingdom,[19] respectively).

(a) Vertical velocity of solid phase (Us,z) at $Z = 0.15$ m; (b) vertical velocity of solid phase (Us,z) at $Z = 0.25$ m; (c) RMS of lateral solid velocity fluctuation (Us,x') at $Z = 0.15$ m; (d) RMS of vertical solid velocity fluctuation (Us,z') at $Z = 0.25$ m; (e) RMS of lateral solid velocity fluctuation (Us,x') at $Z = 0.25$ m; (f) RMS of vertical solid velocity fluctuation (Us,z') at $Z = 0.25$ m.

[Color figure can be viewed in the online issue, which is available at wileyonlinelibrary.com.]

variables. For the velocity, large spouting velocity is applied for the central inlet while a background gas is introduced from other areas of the bottom. Moreover, the constant pressure is assumed at the outlet. Nonslip boundary condition is chosen for the walls of the geometry.

As has been pointed out by Tsuji et al.,[14] the time step adopted for the calculation should be small enough to truly resolve the contacting procedure between colliding particles and make the calculation stable. For the soft-sphere model adopted in the current work, it is assumed that all the energy in a collision procedure is transferred by the Rayleigh waves.[45] Thus, the time step for the solid motion should be smaller than the Rayleigh time, which is the time taken by the Rayleigh wave to propagate along a particle.[45,46] In the dense flow system, the Rayleigh time t_r is evaluated by the correlation as[45]

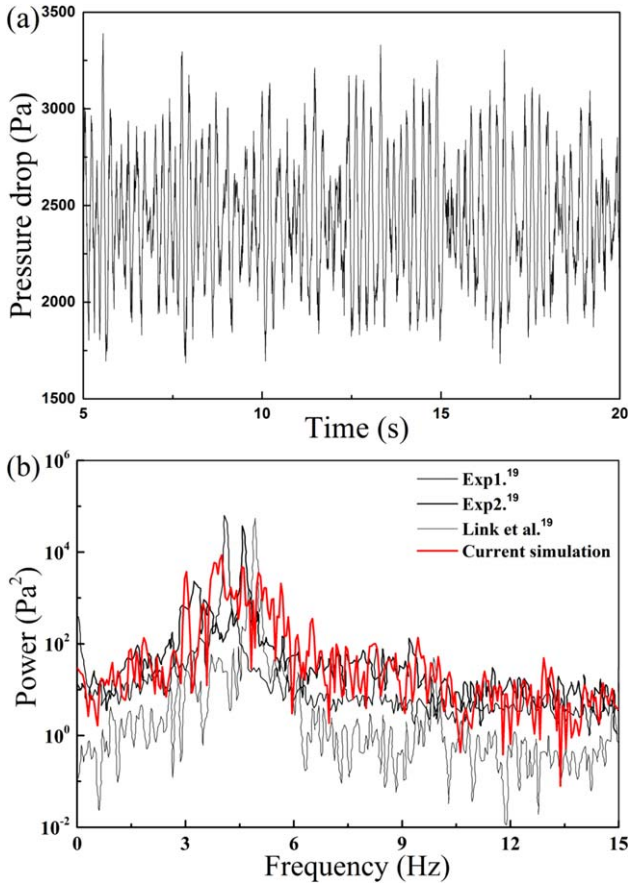

Figure 4. Profiles of pressure drop and its spectral analysis in the time interval of 5–20 s.

(a) Pressure drop profile; (b) comparison of the spectral analysis of pressure drop between the calculated results and the experimental data.[19]

[Color figure can be viewed in the online issue, which is available at wileyonlinelibrary.com.]

$$t_r = \frac{\pi R_p}{0.1631\upsilon_p + 0.8766}\sqrt{\frac{\rho_p}{G_p}} = \frac{\pi R_p}{0.1631\upsilon_p + 0.8766}\sqrt{\frac{2\rho_p(1+\upsilon_p)}{Y_p}} \tag{18}$$

Here, ρ_p and R_p are, respectively, the density and radius of particle p. G_p, Y_p, and υ_p stand for the shear modulus, the Young's modulus, and the Poisson ratio of solid phase, respectively. In the current work, the time step for solid motion is adopted to be 1×10^{-7} s, which is smaller than 0.1 t_r. As has been suggested by Tsuji et al.,[14] the critical time step for the solid motion is much smaller than that of fluid motion from the viewpoint of the stability of calculation. In the simulation, the time step of gas motion is chosen as 1×10^{-5} s. Thus, the coupling between gas and solid phase occurs at every 100 steps of solid motion. Total 20 physical seconds are performed with the hydrodynamics averaged over the calculated results of last 15 s.

Results and Discussion

Sensitivity analysis

As the soft-sphere contact model is used to mimic the interaction procedure between colliding particles, it is important to establish the sensitivity to the numerical parameters adopted in the simulation. In the current work, the settings of related parameters used in the DEM modeling are listed in Table 3. The analysis is carried out by comparing the time-averaged vertical velocity of solid phase at the height of $Z = 0.25$ m. The influence of Young's modulus on the solid vertical velocity is shown in Figure 2a. Even through this parameter decreases from 5×10^{10} to 5×10^{7} Pa, the difference between these cases is small. In a certain range of this parameter, the obtained tendency that the time-averaged property of solid phase is insensitive to the Young's modulus is in accordance with the numerical work of Tsuji et al.[14] in the 2-D fluidized bed and the numerical results of Kuo et al.[47] for the particle behavior in a V-mixer. However, large Young's modulus requires a small time step to capture the collision procedure. Thus, for all the cases involved in the current work, the Young's modulus equaling to 5×10^{8} Pa is adopted. Figure 2b illustrates the influence of Poisson ratio on the solid velocity. It can be found that the variation of Poisson ratio has little influence on solid motion. However, the solid motion in the bed is sensitive to the restitution coefficient, which can be obtained from the velocity distribution shown in Figure 2c. The prediction using small restitution coefficient gives a vigorous motion of solid phase in the bed, which agrees with the influence of restitution coefficient on the solid motion in the conical spouted bed.[48] In all these investigated cases, the simulation with restitution coefficient of 0.95 is chosen to study the topic of current work as the simulated results of this case give better agreement with the experimental data. Figure 2d presents the effect of friction coefficient on the solid motion. It can be observed that the solid vertical velocity with varying friction

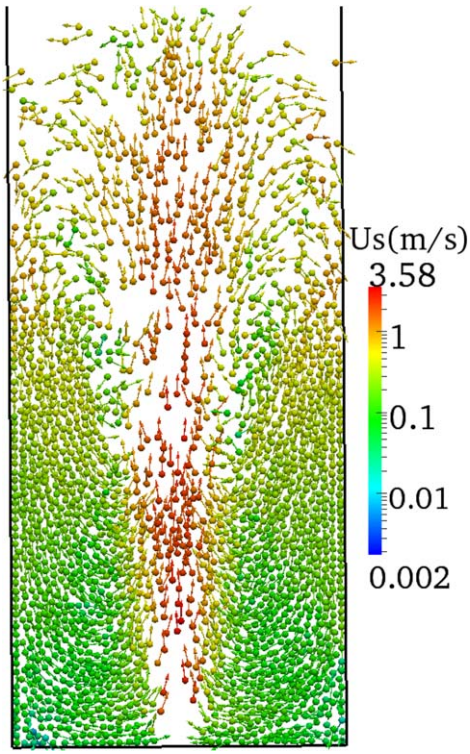

Figure 5. Instantaneous distribution of particles in the slice $Y = 0.042$ m at time instant $t = 11.5$ s (Us is solid velocity, m/s).

[Color figure can be viewed in the online issue, which is available at wileyonlinelibrary.com.]

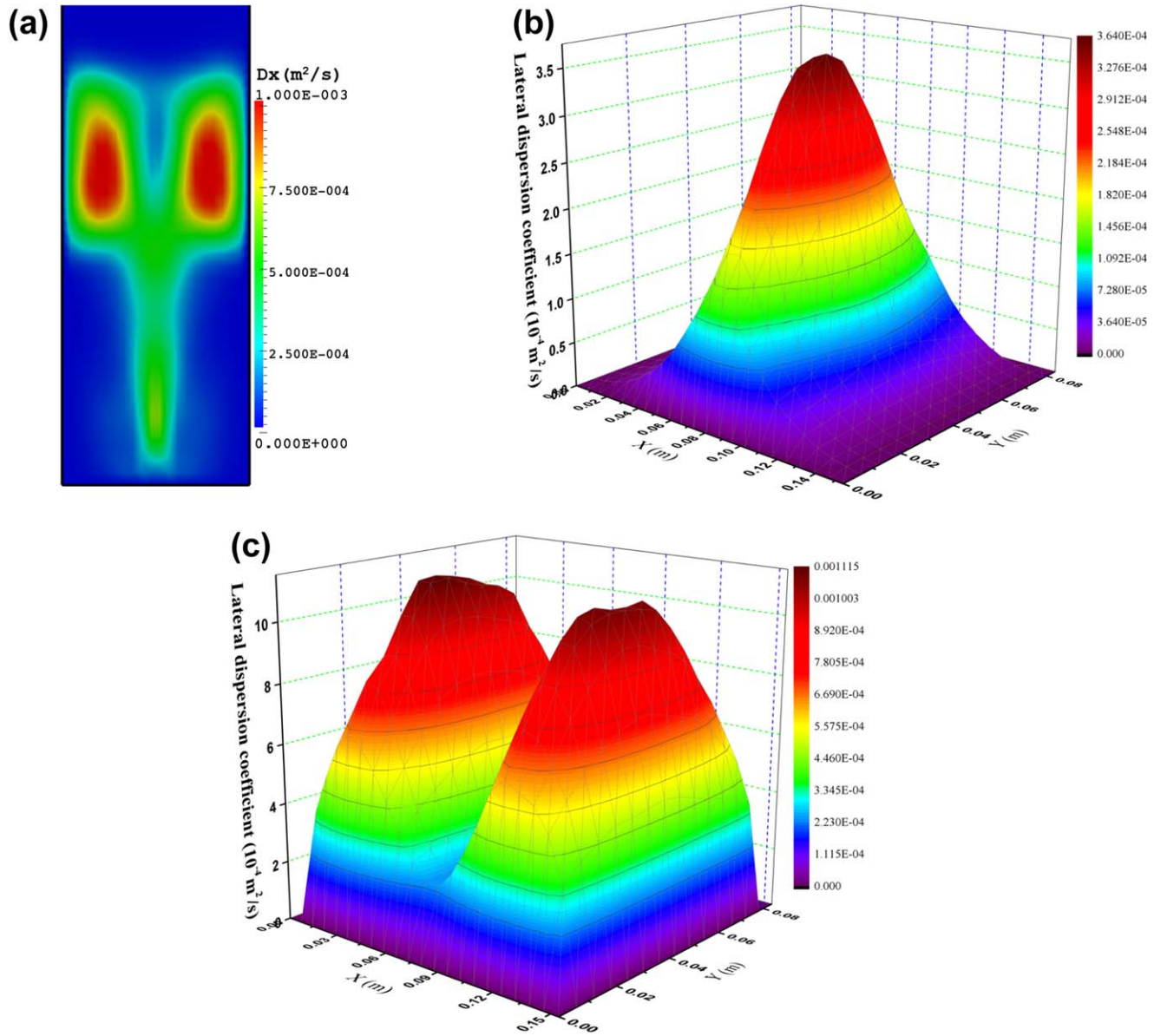

Figure 6. Distribution of time-averaged lateral solid dispersion (Dx, m^2/s) in the system.

(a) Contour plot in $Y = 0.042$ m; (b) surface plot at $Z = 0.15$ m; (c) surface plot at $Z = 0.25$ m.

[Color figure can be viewed in the online issue, which is available at wileyonlinelibrary.com.]

coefficient from 0.1 to 0.25 changes little along the transverse direction. However, obvious difference appears when the friction coefficient equals to 0.3. In the numerical simulation, the dynamical rolling friction is adopted to mimic the behavior of not perfectly spherical particles.[22] As illustrated in Figure 2e, the addition of rolling friction gives rise to better simulation results as compared with the case without this parameter. This tendency agrees well with the numerical results obtained in the spout-fluid bed by Goniva et al.[22] and the simulation carried out in conical spouted bed by Lan et al.[49]

Model validation

As shown in the panels a–f of Figure 3, comparisons of the current numerical results with the experimental data and the simulation conducted by Link et al.[19] are focused on the time-averaged velocity of solid phase and its RMS. In general, the simulation results with three different grid resolutions agree well with the experimental data. At the height of $Z = 0.15$ m locating in the annulus and the spout channel, vigorously vertical motion of solid phase appears in the central region of the bed, while slow downward motion exists in the annulus region. The largest RMS of solid velocity fluctuation along the lateral and vertical directions can be obtained in the spout region, while small velocity fluctuation appears in the annulus due to the motionless status of solid phase. In the fountain, as shown in Figure 3b, particles injected from the spout move energetically in the central part of this region and fall in the periphery of fountain. Conversely, more smooth decreasing tendency of solid velocity along the transverse direction can be observed as compared with that below the bed surface. Across the bed width, the velocity fluctuations in both lateral and vertical directions exhibit more uniform distribution in the fountain region as compared with those at the height of $Z = 0.15$ m. Moreover, the grid-independent study is conducted to investigate the effect of

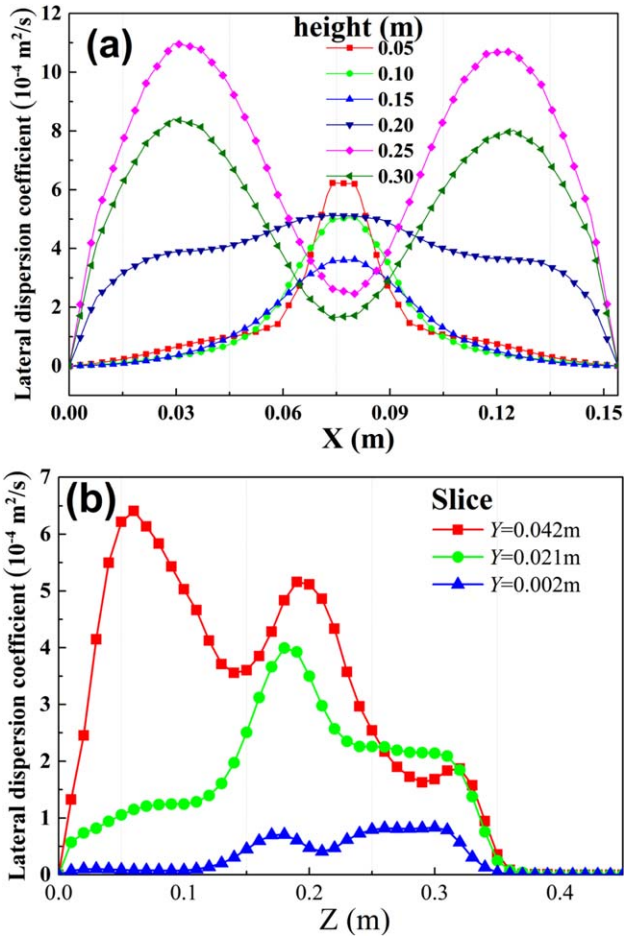

Figure 7. Quantitative comparison of time-averaged lateral dispersion coefficient of solid phase.

(a) Comparison at different heights of $Y = 0.042$ m; (b) comparison in the central lines of three slices along the depth direction.

[Color figure can be viewed in the online issue, which is available at wileyonlinelibrary.com.]

grid resolution on the results obtained from the coupling model. Three test cases are simulated with the geometry divided into 13,600, 20,520, and 29,400, respectively. The results with different grid resolutions are shown in Figure 3. It can be observed that all the grid resolutions give the similar distribution profiles of the time-averaged velocity and its RMS, indicating that the calculation results are independent of grid resolution. The calculated case with a fine grid resolution is adopted to study the related content in the following work.

In addition, the cross-sectional averaged pressure drop and its spectral analysis of the last 15 s, which reflect the dynamical behavior of the bed, are presented in Figure 4. It can be observed that the trend of the frequency spectrum of the calculated pressure drop is in agreement with the measured values. The peak of the profile occupies the frequency range of 4–6 Hz, reflecting that the system operates in the spout-fluidization regime.[19]

These comparisons indicate that the proposed model captures the important dynamic behavior of the system. The remaining difference between the experimental data and the simulated results is mainly due to the two aspects. One aspect is that the predicted motion of solid phase has a strong dependence on the accuracy of the drag force model. However, the adopted drag force model is obtained from the empirical correlation for bed pressure.[38] The other aspect is due to that the solid property is in a range in the practical operation, such as the particle diameter estimated experimentally ranges from 4.02 to 4.06 mm.[19] However, in the calculation procedure, all the particles are set with the same value. Thus, this also raises some difference between the simulated results and experimental data. However, the calculated results agree with the experimental data qualitatively and no systematic difference between them. Hence, it can be adopted to study the dispersion and resident properties of current system.

General solid flow behavior

The investigated case is operated in the spout-fluidization regime (Case B1 of Link et al.[19]), in which an intermittent spout channel is formed in the system and occasionally penetrates through the whole spout region, while sometimes it is blocked by the particles falling from the upper annulus region. Excellently circulating behavior of solid phase is established in the system after the start-up procedure. Solid movement behavior at the same time instant is shown in Figure 5. Three typical regions with significantly different movement behaviors of solid phase can be observed. Particles rise upward vigorously in the spout region with small solid concentration, and then are injected into the fountain region after the spout outlet is reached. Subsequently, particles cascade and settle on the bed surface, followed by a slow downward movement in the annulus. Meanwhile, it can be clearly observed that the particles are entrained into the spout region from spout-annulus interface along the axial direction in the falling process, which will obviously influence the distribution characteristic of SRT in the spout region.

Lateral dispersion property

Qualitative distribution of lateral dispersion coefficient of solid phase in the system is illustrated in Figure 6. The intensively lateral dispersion of solid phase in the periphery of fountain region and spout region reflects the strong lateral mixing of solid phase in these two regions, which mainly corresponds to the lateral motion of particles after injected from spout and the random falling of solid phase from annulus to spout along the axial direction, respectively. Markedly distinct dispersion behavior of solid phase is captured in the spout and fountain regions by comparing the surface plots shown in Figure 6. Moreover, the effect of inlet configuration on solid lateral dispersion can be noted from the surface plots shown in Figures 6b, c. Due to the smaller size of the depth compared with the bed width, the peaks of solid dispersion coefficient in the spout and fountain regions have a wider distribution along the depth direction. Meanwhile, lateral solid dispersion near the wall exhibits different behaviors in different regions of the system. In the annulus, as shown in Figure 6b, more smooth lateral dispersion exists in the vicinities of the left and right walls as compared with that near the front and back walls as more flow area are available for solid motion. However, the sharply decreasing tendency of solid lateral dispersion can be obtained in the near wall region of the fountain.

Comparison of the distribution profiles of lateral solid dispersion in the bed can be used to quantitatively investigate

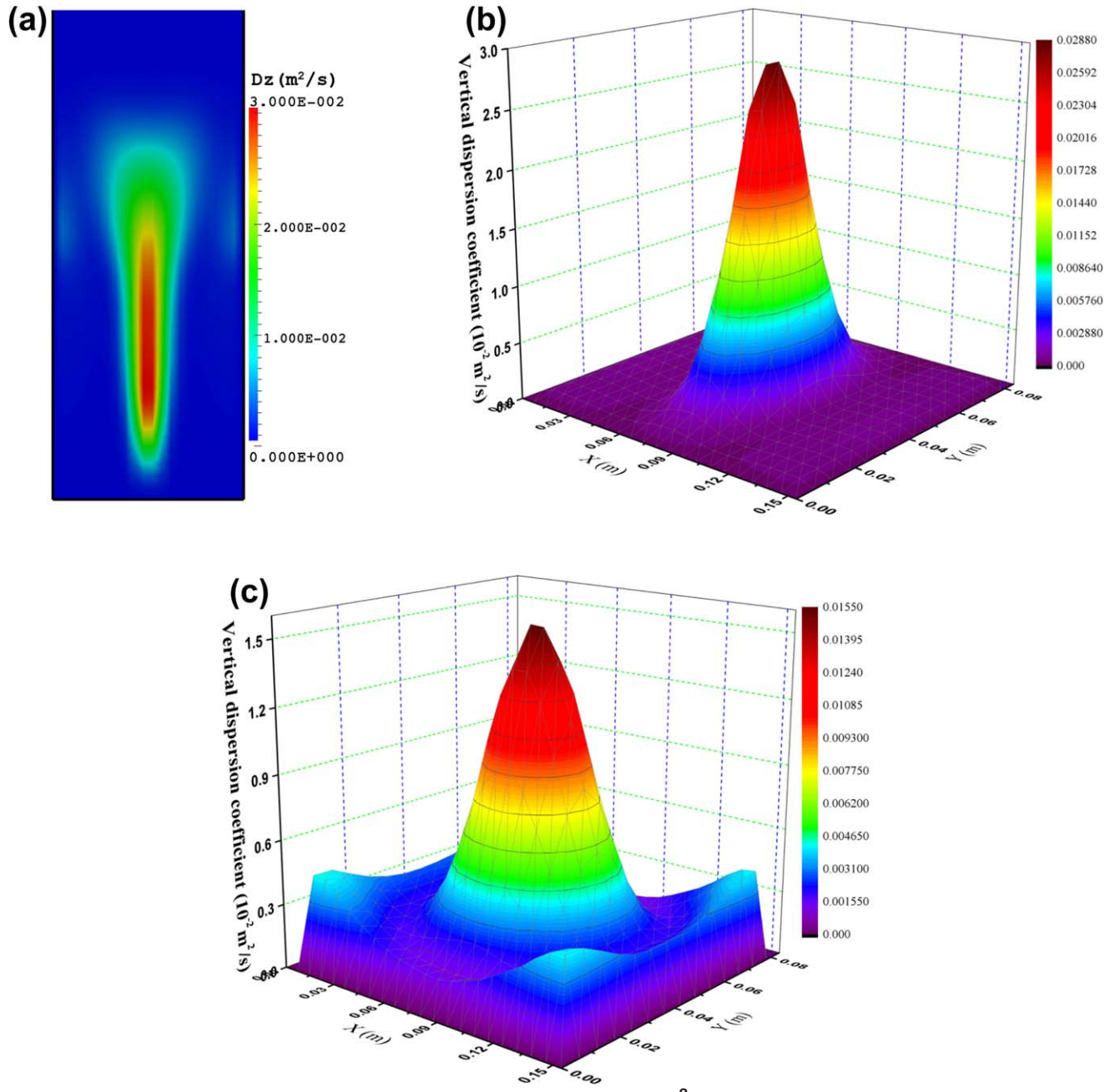

Figure 8. Distribution of time-averaged vertical solid dispersion (*Dz*, m^2/s) in the system.

(a) Contour plot in the slice of $Y = 0.042$ m; (b) surface plot at $Z = 0.15$ m; (c) surface plot at $Z = 0.25$ m.

[Color figure can be viewed in the online issue, which is available at wileyonlinelibrary.com.]

the variation tendency of the solid mixing rate in the transverse direction. Figure 7a illustrates the distribution profiles of lateral solid dispersion in the central plane of $Y = 0.042$ m. In the central region of the bed, the variation tendency of lateral dispersion intensity reflects that the lateral mixing rate of solid phase increases greatly with the bed elevation and then decreases in the fountain region. Vigorous lateral dispersion of solid phase in the spout region is mainly due to the continuous entrainment of particles from annulus to spout and the dilute distribution of particles. However, the lateral dispersion intensity of solid phase in the annulus exhibits little variation with bed elevation due to the loosely packed status of solid motion. Along the central lines of three slices across the depth direction, the lateral mixing rate of solid phase decreases from central region to the near wall region, mainly due to the mutual effect of contact-dominated flow characteristic and the wall limitation on the solid lateral motion.

Vertical dispersion property

Due to the vertical introduction of gas phase, significant vertical dispersion behavior of solid phase appears as compared with the lateral one. Qualitative illustration of the solid vertical dispersion behavior in the system is shown in Figure 8. In a macroscopic view, vigorously vertical dispersion of solid phase exists in the central region of the system, which is due to the energetic motion of gas phase and dilute distribution of solid phase in this region. However, in the annulus region, the

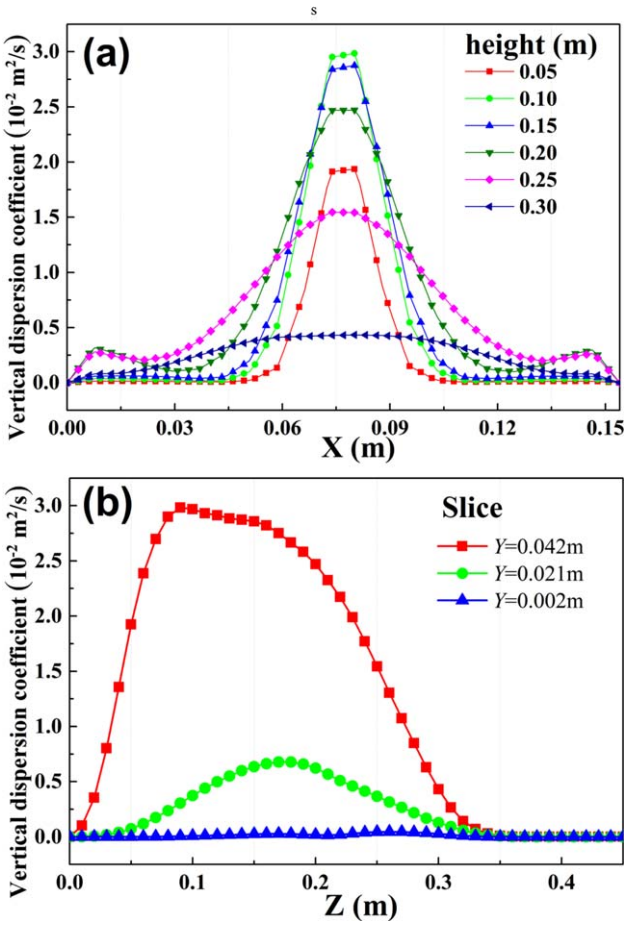

Figure 9. Quantitative comparison of time-averaged vertical dispersion coefficient of solid phase.

(a) Comparison at different heights in slice $Y = 0.042$ m; (b) comparison in the central lines of three slices along the depth direction.

[Color figure can be viewed in the online issue, which is available at wileyonlinelibrary.com.]

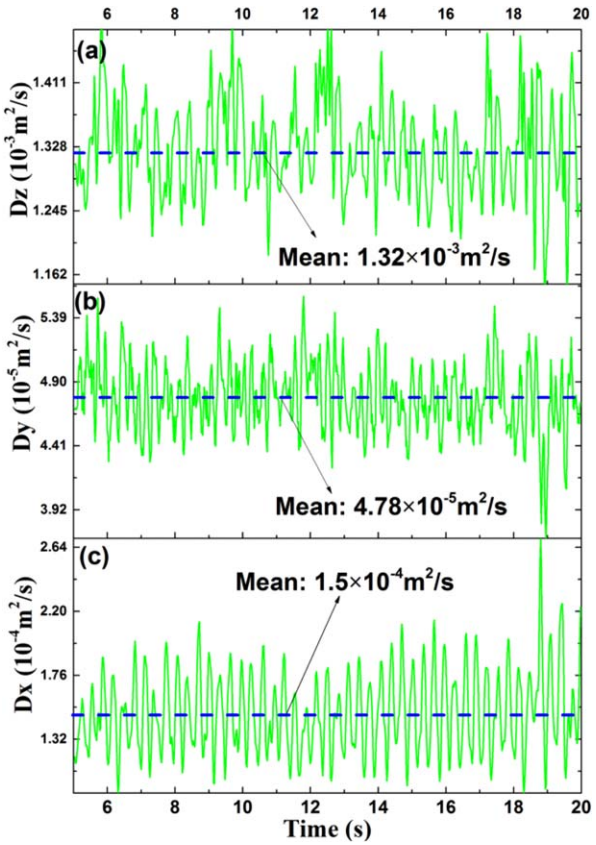

Figure 10. Time evolutionary profiles of systematic dispersion coefficients of solid phase in three directions.

(a) Dispersion in the vertical direction (*Dz*); (b) dispersion in the depth direction (*Dy*); (c) dispersion in the width direction (*Dx*).

[Color figure can be viewed in the online issue, which is available at wileyonlinelibrary.com.]

vertical dispersion of solid phase is not obvious, mainly due to the motionless status of solid phase in the falling procedure. The inlet configuration has a strong influence on the vertical solid dispersion below the bed surface, leading to the larger distribution size along the depth direction. However, this influence disappears in the fountain region, as illustrated in Figure 8c, as more uniform dispersion behavior can be captured in the central region. Besides, vigorously vertical dispersion behavior appears in the vicinity of the bed walls, resulting from the falling of particles in this region of the fountain.

Figure 9a shows the quantitative description of the vertical dispersion intensity in slice $Y = 0.042$ m. The initial increase of vertical dispersion coefficient in the central region is mainly due to the energetic momentum transferred from gas phase to particles and the dilute concentration of solid phase in the spout region. Along the vertical direction, gas leakage from central region to its surrounding lowers the momentum transferred to the upward particles, which reduces the vertical mixing rate of solid phase. Moreover, small change of solid vertical dispersion intensity appears in the annulus region due to the frequent collision between particles. Along the axial direction, as shown in Figure 9b, vigorously vertical dispersion of solid phase exists in slices $Y = 0.042$ m and $Y = 0.021$ m, mainly resulting from the vigorous gas motion and relatively dilute distribution of solid phase. Correspondingly, the vertical dispersion of solid phase in slice $Y = 0.002$ m is not obvious due to the frequent collision between particles. In addition, the strongest vertical dispersion in the central slice of $Z = 0.042$ m reaches the maximum value below the spout outlet, resulting from the reduced gas momentum and the frequently choking of particles from upper annulus to spout in the spout-fluidization flow regime.

Systematic dispersion behavior

The spatial distribution of solid dispersion coefficient reflects only the local dispersion property in the system. As mentioned above, not only different dispersion behaviors exist in the different regions of the spout-fluid bed, but also the dispersion intensity shows significantly different scale. Hence, systematic dispersion coefficient of solid phase is adopted as a global parameter to reflect the dispersion behavior of the whole system in a macroscopic view and a criterion to compare the influences of operating parameters, such as superficial velocity and particle diameter, on dispersion property of the system.

Figure 10 demonstrates the time evolutionary profiles of the systematic dispersion coefficients in all three directions after the bed reaching the stable operation. It is observed that all

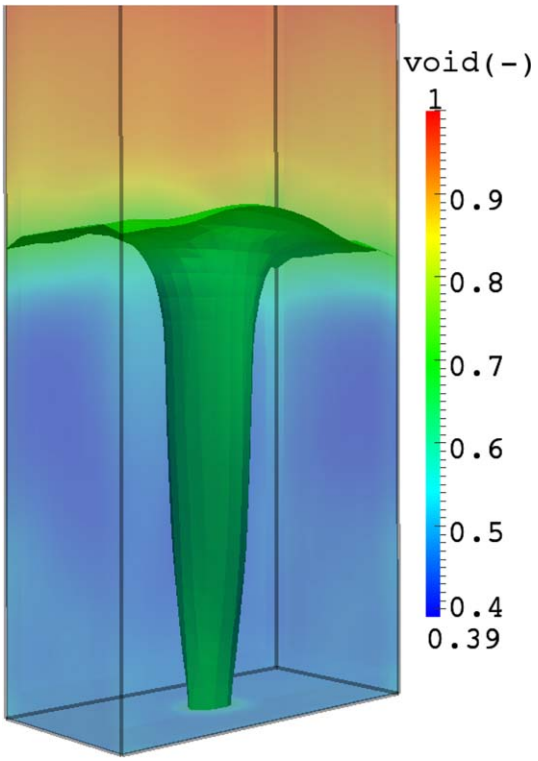

Figure 11. 3-D view of the spout-annulus interface in the spout-fluid bed (identified with a threshold voidage of 0.65).

[Color figure can be viewed in the online issue, which is available at wileyonlinelibrary.com.]

the dispersion coefficients fluctuate around a constant value, which is due to the chaotic and turbulent properties of the gas–solid system. The averaged systematic dispersion coefficients of solid phase in X, Y, and Z directions are equal to 1.5 $\times$ 10^{-4}, 4.78 $\times$ 10^{-5}, and 1.32 $\times$ 10^{-3} m^2/s, respectively, which reflect the anisotropy of solid mixing rate along the three directions of the system. The vertical mixing rate of solid phase is nearly stronger at one order magnitude than the lateral one since the vertical direction is the main flow direction. This is in accordance with the experimental work of Zhang et al.[34] Meanwhile, dispersion intensity in the depth direction is the weakest, mainly due to strong restriction of wall effect on the solid motion. Hence, the influence of inlet configuration on the systematic dispersion behavior is obvious. With the width is larger nearly as twice as that in the depth

Table 4. Comparison of Mean and Standard Deviation of Solid Dispersion Coefficients in Three Regions of System

Region	Direction	Mean of Solid Dispersion Coefficient (10^{-4} m^2/s)	Standard Variation of Solid Dispersion Coefficient (10^{-4} m^2/s)
Spout	X	3.99	1.13
	Y	1.76	0.32
	Z	143.7	9.62
Annulus	X	0.64	0.16
	Y	0.13	0.015
	Z	4.56	0.79
Fountain	X	5.98	1.25
	Y	2.18	0.23
	Z	35.9	5.31

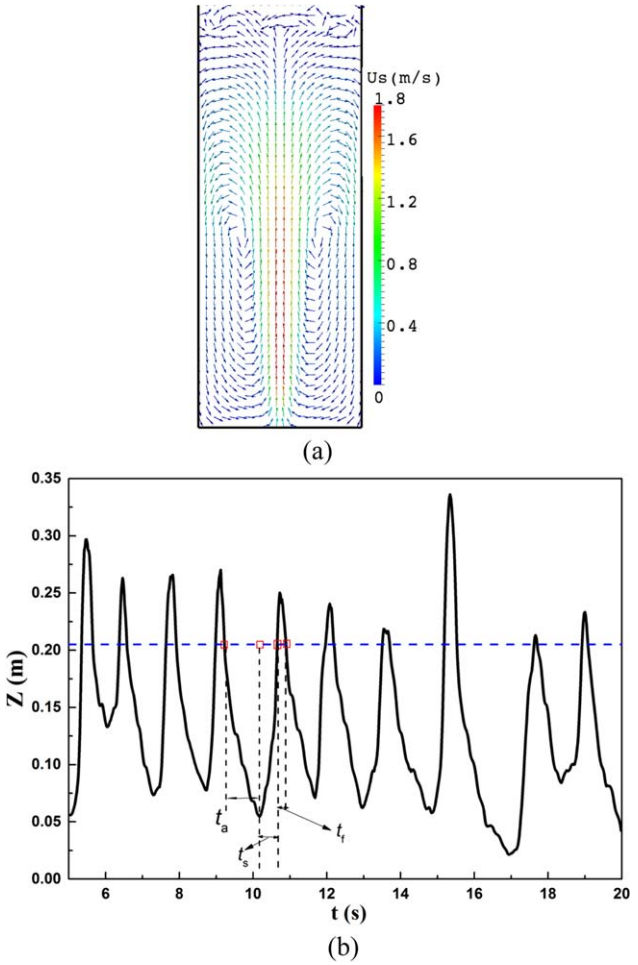

Figure 12. (a) Vector plot of time-averaged solid velocity in slice $Y = 0.042$ m; (b) trajectory of a particle along the Z direction in the time interval 5–20 s (t_s, t_a, and t_f stand for the time of the particle elapsing the spout, annulus, and fountain regions, respectively).

[Color figure can be viewed in the online issue, which is available at wileyonlinelibrary.com.]

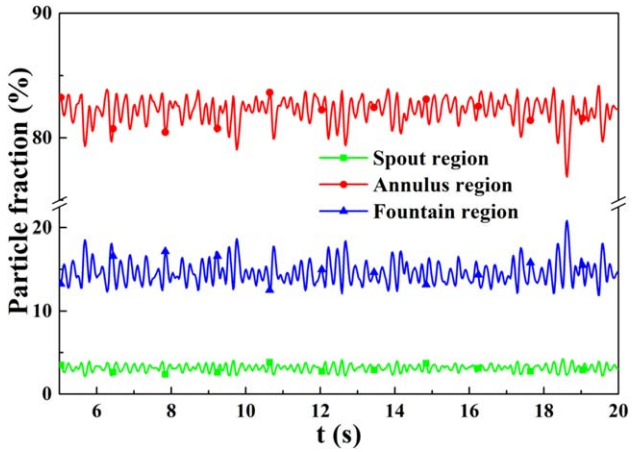

Figure 13. Time evolutionary profiles of particle fraction in the three regions of the spout-fluid bed in the time interval 5–20 s.

[Color figure can be viewed in the online issue, which is available at wileyonlinelibrary.com.]

Table 5. Statistics of the Particle Number Exists in the Three Regions of the Spout-Fluid Bed

Regions	Fraction Occupied (%)	Mean Particle Number	Standard Variation
Spout	2.9	1305	163
Annulus	82.5	36,923	445
Fountain	14.6	6570	585

direction, the solid dispersion intensity along the width direction is several time of that along the depth direction.

The existence of three regions with significant distinct flow characteristics results in the different dispersion intensities among them. Initially, the system is divided into three regions with the iso-surface of voidage equaling to 0.65, as demonstrated in Figure 11. Correspondingly, all the particles involved are divided into three groups. At each time instant, the dispersion coefficient of solid phase in each region is averaged over all the dispersion coefficients of particles locating in this region. Then, an average value is obtained by averaging over the data of all the time instants. The dispersion intensities of solid phase in all three regions are listed in Table 4. For all the three components, the dispersion intensity of solid phase in the annulus region is the smallest due to its contact-dominated flow characteristics. The strongest dispersion intensity of solid phase along the vertical direction appears in the spout region as the drag force exerted on a particle is greater than its gravity and the particles in this region distribute sparsely.

Solid circulation pattern

Solid circulating property can be used to identify the motion pattern of solid phase in the spout-fluid bed. Vector plot of the time-averaged solid velocity in slice $Y = 0.042$ m is illustrated in Figure 12a. It can be clearly observed that solid circulation is mainly achieved through two circulating rolls locating in the periphery of the bed. By means of particle-scale simulation, the trajectory of a specific particle in the system is tracked in the whole calculation procedure. Figure 12b presents the time evolution of particle position along the vertical direction. Regular movement can be found and two circulating patterns can be identified for the solid transportation, namely the gross circulation and the local circulation. In a gross circulation pattern, the particle is dragged upward vigorously by the gas phase until the maximum height is reached. Then, a falling procedure appears under the influence of gravity. After the bed surface is touched, a downward movement appears with solid velocity decreasing in the falling process. When the bed bottom is arrived, the whole gross circulation is finished. Occasionally, in the falling procedure, lots of particles are entrained into the spout region from spout-annulus interface, leading to the formation of local circulation pattern.

The continuous operation of whole system needs the pseudosteady operation established in these three regions. By means of the approach used to evaluate the solid dispersion intensity in each region, the instantaneous number of particles in each region is recorded at each time instant. Figure 13 illustrates the time evolutionary profiles of particle fraction in these three regions. The time-averaged values of particle fraction in these three regions are listed in Table 5. In general, nearly 2.9% of particles locate in the spout region, whereas nearly 82.5% of them are in the annulus region. This property quantifies the fraction of the particles locating in different regions of system, which is extremely useful for

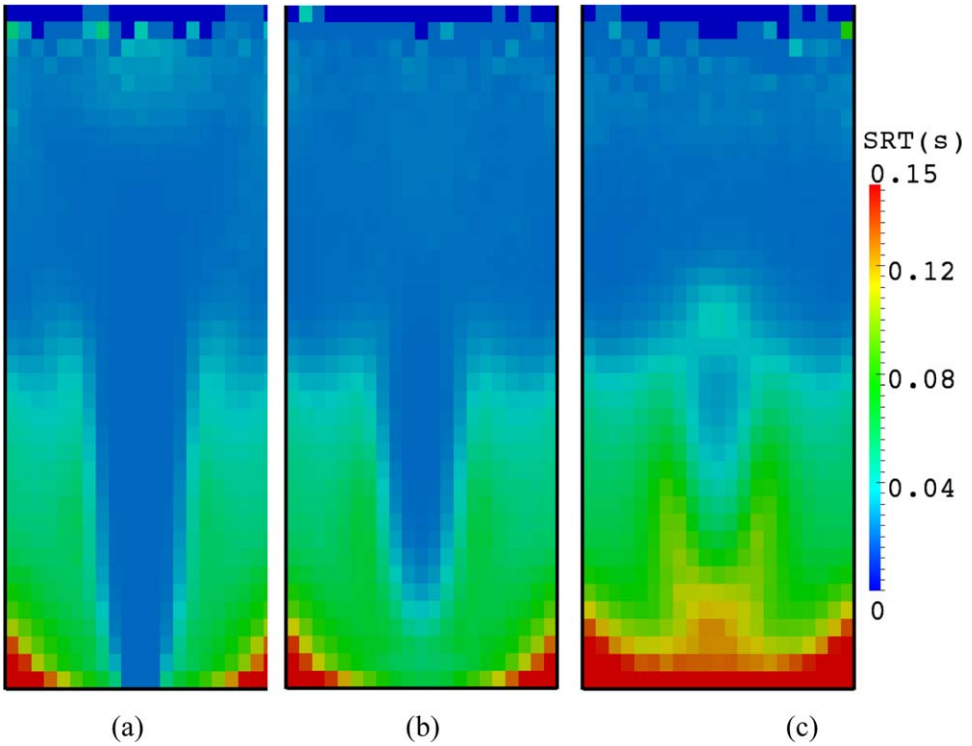

Figure 14. Snapshots of local SRT distributions in three slices along the depth direction (sampling frequency is 1000 Hz and total sampling time is 2 s).

(a) $Y = 0.042$ m; (b) $Y = 0.021$ m; (c) $Y = 0.002$ m.

[Color figure can be viewed in the online issue, which is available at wileyonlinelibrary.com.]

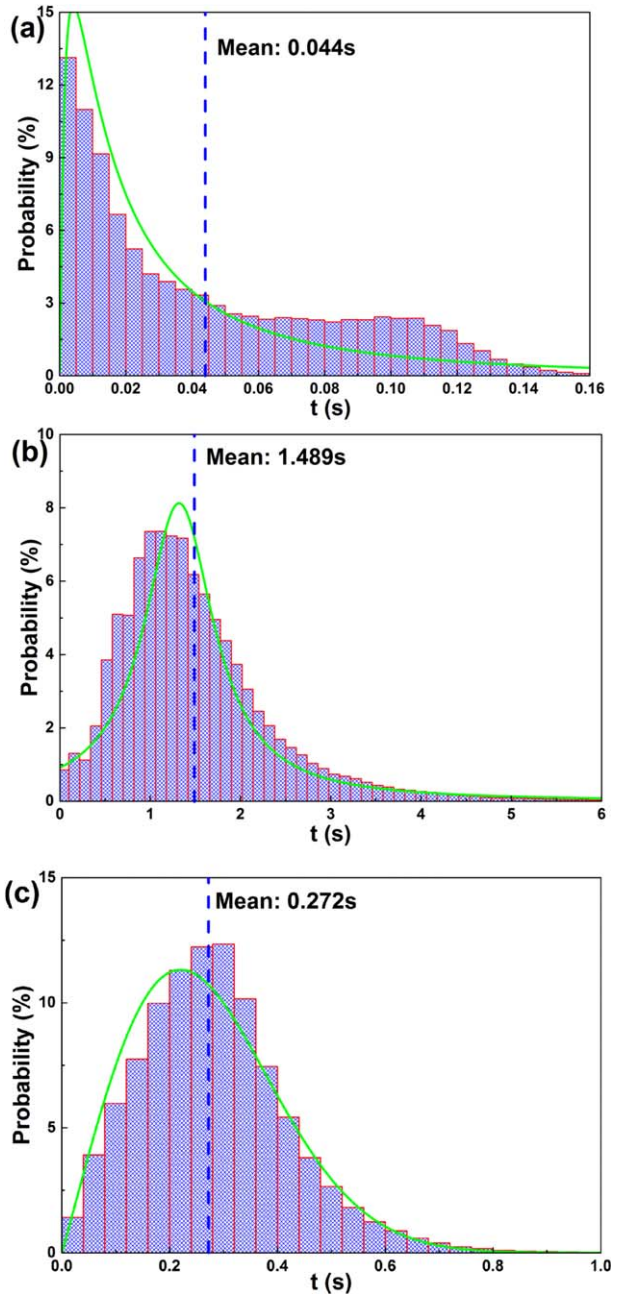

Figure 15. Probability histograms of the SRTs in the three regions of spout-fluid bed.

(a) SRT distribution in the spout; (b) SRT distribution in the annulus; (c) SRT distribution in the fountain.

[Color figure can be viewed in the online issue, which is available at wileyonlinelibrary.com.]

the understanding of solid distribution and the design of the apparatus.

Solid residence time

Different local flow characteristic of solid phase in the fluidizing apparatus leads to the different local resident behaviors. Exploring this aspect is useful for obtaining a well-controlled system as some harsh environment, such as hot formation with agglomeration and cohesion, strongly affects the catalyst deactivation in the chemical reactors.

In the current numerical work, local resident behavior of solid phase is quantitatively evaluated with the local SRT. It is obtained by tracking the trajectories of all the particles in the system. In a specific computational grid, local SRT is averaged over all the residence times of the particles passing through the current cell in the calculation time. Figure 14 shows the contour plots of local SRT in three slices of the spout-fluid bed. In slice $Y = 0.042$ m, as illustrated in Figure 14a, it is obviously observed that small SRT appears in the central region, whereas large value appears in the annulus especially the corner of bottom region. In the periphery of the system, SRT diminishes with bed elevation, which indicates that the solid motion becomes slow with the falling in the annulus. From the comparison of distribution plots in the central plane and the other two planes, it can be observed that SRT is enlarged in the whole slice at the vicinity of bed walls. Moreover, large local residence time of solid phase in the fountain mainly appears at the top of this region.

When circulating in the spout-fluid bed, a particle subsequently goes through three regions of the system. Due to the distinct flow characteristics of solid phase in these three region, exploring the resident behaviors of solid phase in three regions of the system is helpful for understanding the solid transportation in the system. The residence time of a specific particle in a specific region is recorded when it crosses the boundaries between these three region. After this particle exits this region, the residence time it elapsed is recorded. Three regions are identified with the approach used to evaluate the solid dispersion intensities in the three regions. The residence times in all the three regions are extracted and averaged separately. The probability histogram distribution of the SRT in each region is shown in Figure 15. It can be observed that SRT mainly concentrates in the time ranges of 0–6 s. The smallest residence time appears in the spout region with an average value of 0.044 s, resulting from the most intense motion of solid phase in this region of the bed. Meanwhile, the SRT in this region distributes with an early-occurred peak and a long tail, mainly due to the frequent falling of particles from the annulus region to spout region along the axial direction. Furthermore, the SRT in the fountain region is 6.18 times of that in the spout region. The largest SRT appears in the annulus region, resulting from the motionless status of solid phase in this region. Besides, the mean SRT in the annulus region is 1.489 s, which is larger than that in the spout region with nearly an order of magnitude. Statistically, the internal circulation of a general particle in this kind of spout-fluid bed operated in the spout-fluidization regime elapses nearly 82.49% of its cycle time in the annulus region, nearly 15.07% of its cycle time in the fountain region, and only 2.44% in the spout region. Quantification of the SRT in three regions is extremely useful for the design and operation of the spout-fluid bed. In addition, the histograms of SRTs in these three regions show different distribution profiles. The current work takes an effort to fit these profiles with the commonly used distribution patterns. As can be observed in Figure 15, the SRTs in the spout, annulus, and fountain regions are well fitted with the log-normal distribution profile, the Lorenz distribution profile, and the normal distribution profile, respectively. The conclusions that the SRTs in these three regions of the spout-fluid bed can be predicted with these three distribution patterns should be widely investigated with more cases of different operating parameters and bed geometrical configuration. By means of the particle-scale investigation, this will be a further study in the following work.

Conclusions

A 3-D CFD-DEM coupling approach is established to simulate the gas–solid flow in a spout-fluid bed. The dispersion and resident behaviors of solid phase are investigated. Based on the calculated results, the following conclusions can be drawn:

1. Vigorously lateral dispersion of solid phase appears in the periphery of the fountain region and the spout region. The inlet geometry has a strong influence on the lateral dispersion behavior of solid phase. Intensively vertical dispersion of solid phase exists in the central region of the system. The influence of inlet geometry on the vertical dispersion behavior is obviously below the bed surface, while this influence disappears in the fountain region.
2. The anisotropy of solid mixing rate along the three directions can be observed. In all the three directions, the vertical dispersion intensity of solid phase is nearly stronger at one order magnitude than the lateral one. Influenced by the inlet configuration, the dispersion intensity of solid phase along the width direction is several times of that along the depth direction. The strongest dispersion intensity of solid phase is observed in the spout.
3. Internal circulation of solid phase is achieved through two circulating rolls locating in the periphery of the bed. Particle-scale investigation of solid transportation indicates that two circulation patterns can be captured, namely the gross circulation and the local circulation. Nearly 82.5% of the total particles locates in the annulus region and only 2.9% of them exists in the spout.
4. Small local SRT is observed in the central spout region, while the residence time in the bottom corner shows the largest. The closer to the wall region, the larger residence time appears. The mean SRT in the annulus is larger than that in the spout with nearly an order of magnitude. Moreover, the SRT in the fountain is several as large as that in the spout.

Acknowledgment

Financial supports from the Major Program of the National Natural Science Foundations of China (Grant Nos. 51390491, 51390493) and the National Program for Special Support of Top-Notch Young Professionals are sincerely acknowledged.

Notations

C_D = drag force coefficient, dimensionless
d_p = particle diameter, m
e = restitution coefficient, dimensionless
D = dispersion coefficient of solid phase, m^2/s
Dx = dispersion coefficient of solid phase in the X direction, m^2/s
Dy = dispersion coefficient of solid phase in the Y direction, m^2/s
Dz = dispersion coefficient of solid phase in the Z direction, m^2/s
$\boldsymbol{F}_c$ = contact force, N
$\mathbf{f}_d$ = drag force, N
$\mathbf{f}_p$ = far field pressure force, N
$\mathbf{g}$ = gravitational acceleration, m/s^2
G = shear modulus of solid phase, Pa
G^* = equivalent shear modulus of solid phase, Pa
$\mathbf{I}$ = a second-order metric tensor, dimensionless
I_p = particle moment of inertia, kg/m^2
k = total number of particles or walls colliding with current particle, dimensionless
$k_{n,ij}$ = normal stiffness coefficient of solid phase, N/m
$k_{t,ij}$ = tangential stiffness coefficient of solid phase, N/m
m_p = particle mass, kg
m^* = effective mass of a particle, kg
N_p = number of particles in the whole system, dimensionless
N_t = total number of the time instants, dimensionless
n = total number of particles locating in a specific cell, dimensionless
$\boldsymbol{n}$ = normal unit vector between colliding particles, dimensionless
n_j = total number of particles locating in a specific cell at time instant j, dimensionless
p_g = pressure, Pa
r = particle position, m
Δr = particle displacement, m
R_p = particle radius, m
R^* = effective radius of a particle, m
Re_p = particle Reynolds number, dimensionless
S_n = normal stiffness, N/m
S_t = tangential stiffness, N/m
$\boldsymbol{T_p}$ = torque exerted on a particle, N/m
Δt = time step, s
t = time instant, s
t_a = time required for a particle to pass the annulus region, s
t_f = time required for a particle to pass the fountain region, s
t_r = Rayleigh time, s
t_s = time required for a particle to pass the spout region, s
$\boldsymbol{t}$ = tangential unit vector between colliding particles, dimensionless
$\mathbf{u}_g$ = gas velocity in the current cell, m/s
$\mathbf{U}_s$ = solid velocity, m/s
$U_{s,x}$ = velocity component in the X-coordinates, m/s
$U_{s,z}$ = velocity component in the Z-coordinates, m/s
$U_{s,x'}$ = RMS of lateral solid velocity fluctuation, m/s
$U_{s,z'}$ = RMS of vertical solid velocity fluctuation, m/s
$\boldsymbol{v}_{n,ij}$ = normal component of relative velocity between colliding pair, m/s
$\boldsymbol{v}_{t,ij}$ = tangential component of relative velocity between colliding pair, m/s
$\boldsymbol{v}_p$ = particle velocity, m/s
$V_{pi,t}$ = total volume of elements of particle i in a specific cell, m^3
V_p = particle volume, m^3
ΔV = volume of the current cell, m^3
X = slice position in the X-coordinates, m
Y = slice position in the Y-coordinates, m
Y_p, Y^* = actual and effective Young's modulus, Pa
Z = slice position in the Z-coordinates, m

Greek symbols

β = interphase momentum transfer coefficient, $kg/(m^3\ s)$
δ_{nij} = normal displacement between particle i and particle j, m
δ_{tij} = tangential displacement between particle i and particle j, m
ε_g = voidage, dimensionless
λ_g = bulk viscosity of fluid phase, kg/(m s)
μ_g = shear viscosity of fluid phase, kg/(m s)
μ_p = friction coefficient between particles or particle-wall, dimensionless
μ_{df} = dynamical friction coefficient between particles or particle-wall, dimensionless
ψ = damping ratio, dimensionless
ρ_g = gas density, kg/m^3
ρ_p = particle density, kg/m^3
ω_p = particle angular velocity, 1/s
γ_n = damping coefficient in normal direction, kg/s
γ_t = damping coefficient in tangential direction, kg/s
τ_g = stress tensor of fluid phase, Pa
v = Poisson ratio of solid phase, dimensionless

Subscripts

c = contact force
g = gas phase
i = particle i

j = particle j
n = normal component of a variable
p = particle phase
t = tangential component of a variable

Abbreviations

2-D = two-dimensional
3-D = three-dimensional
CFD = computational fluid dynamics
DEM = discrete element method
DRF = dynamical rolling friction
PR = Poisson ratio
RMS = root mean square
SRT = solid residence time

Literature Cited

1. Zielinska M, Markowski M. Drying behavior of carrots dried in a spout–fluidized bed dryer. *Dry Technol*. 2007;25:261–270.
2. Kfuri CR, Freitas L. A comparative study of spouted and spout-fluid beds for tablet coating. *Dry Technol*. 2005;23:2369–2387.
3. Lim CJ, Watkinson AP, Khoe GK, Low S, Epstein N, Grace JR. Spouted, fluidized and spout-fluid bed combustion of bituminous coals. *Fuel*. 1988;67:1211–1217.
4. Thamavithya M, Dutta A. An investigation of MSW gasification in a spout-fluid bed reactor. *Fuel Process Technol*. 2008;89:949–957.
5. Sutkar VS, Deen NG, Kuipers JAM. Spout fluidized beds: recent advances in experimental and numerical studies. *Chem Eng Sci*. 2013;86:124–136.
6. Patterson EE, Halow J, Daw S. Innovative method using magnetic particle tracking to measure solids circulation in a spouted fluidized bed. *Ind Eng Chem Res*. 2009;49:5037–5043.
7. Zhong W, Zhang M. Characterization of dynamic behavior of a spout-fluid bed with Shannon entropy analysis. *Powder Technol*. 2005;159:121–126.
8. Zhong W, Zhang M, Jin B. Maximum spoutable bed height of spout-fluid bed. *Chem Eng J*. 2006;124:55–62.
9. Zhong W, Xiao R, Zhang M. Experimental study of gas mixing in a spout-fluid bed. *AIChE J*. 2006;52:924–930.
10. van Buijtenen MS, Börner M, Deen NG, Heinrich S, Antonyuk S, Kuipers JAM. An experimental study of the effect of collision properties on spout fluidized bed dynamics. *Powder Technol*. 2011;206:139–148.
11. Hou QF, Zhou ZY, Yu AB. Computational study of heat transfer in a bubbling fluidized bed with a horizontal tube. *AIChE J*. 2012;58:1422–1434.
12. Feng YQ, Xu BH, Zhang SJ, Yu AB, Zulli P. Discrete particle simulation of gas fluidization of particle mixtures. *AIChE J*. 2004;50:1713–1728.
13. Zhou ZY, Kuang SB, Chu KW, Yu AB. Discrete particle simulation of particle–fluid flow: model formulations and their applicability. *J Fluid Mech*. 2010;661:482–510.
14. Tsuji Y, Kawaguchi T, Tanaka T. Discrete particle simulation of two-dimensional fluidized bed. *Powder Technol*. 1993;77:79–87.
15. Zhou ZY, Yu AB, Zulli P. Particle scale study of heat transfer in packed and bubbling fluidized beds. *AIChE J*. 2009;55:868–884.
16. Yang S, Luo K, Fang M, Zhang K, Fan J. Three-dimensional modeling of gas–solid motion in a slot-rectangular spouted bed with the parallel framework of the computational fluid dynamics–discrete element method coupling approach. *Ind Eng Chem Res*. 2013;52:13222–13231.
17. Fang M, Luo K, Yang S, Zhang K, Fan J. LES-DEM investigation of gas–solid flow dynamics in an internally circulating fluidized bed. *Chem Eng Sci*. 2013;101:213–227.
18. Link JM, Godlieb W, Deen NG, Kuipers JAM. Discrete element study of granulation in a spout-fluidized bed. *Chem Eng Sci*. 2007;62:195–207.
19. Link JM, Deen NG, Kuipers J, Fan X, Ingram A, Parker DJ, Wood J, Seville J. PEPT and discrete particle simulation study of spout-fluid bed regimes. *AIChE J*. 2008;54:1189–1202.
20. Zhang Y, Jin B, Zhong W, Ren B, Xiao R. DEM simulation of particle mixing in flat-bottom spout-fluid bed. *Chem Eng Res Des*. 2010;88:757–771.
21. van Buijtenen MS, Buist K, Deen NG, Kuipers JAM, Leadbeater T, Parker DJ. Numerical and experimental study on spout elevation in spout-fluidized beds. *AIChE J*. 2012;58:2524–2535.
22. Goniva C, Kloss C, Deen NG, Kuipers JAM, Pirker S. Influence of rolling friction on single spout fluidized bed simulation. *Particuology*. 2012;10:582–591.
23. Olsson J, Pallarès D, Johnsson F. Lateral fuel dispersion in a large-scale bubbling fluidized bed. *Chem Eng Sci*. 2012;74:148–159.
24. Liu D, Chen X. Quantifying lateral solids mixing in a fluidized bed by modeling the thermal tracing method. *AIChE J*. 2012;58:745–755.
25. Chalermsinsuwan B, Gidaspow D, Piumsomboon P. Two- and three-dimensional CFD modeling of Geldart A particles in a thin bubbling fluidized bed: comparison of turbulence and dispersion coefficients. *Chem Eng J*. 2011;171:301–313.
26. Liu D, Chen X. Lateral solids dispersion coefficient in large-scale fluidized beds. *Combust Flame*. 2010;157:2116–2124.
27. Pallarès D, Johnsson F. A novel technique for particle tracking in cold 2-dimensional fluidized beds—simulating fuel dispersion. *Chem Eng Sci*. 2006;61:2710–2720.
28. Luo K, Yang S, Zhang K, Fang M, Fan J. Particle dispersion and circulation patterns in a 3D spouted bed with or without draft tube. *Ind Eng Chem Res*. 2013;52:9620–9631.
29. Di Benedetto A, Russo P, Sanchirico R, Di Sarli V. CFD simulations of turbulent fluid flow and dust dispersion in the 20 liter explosion vessel. *AIChE J*. 2013;59:2485–2496.
30. Di Sarli V, Russo P, Sanchirico R, Di Benedetto A. CFD simulations of dust dispersion in the 20 L vessel: effect of nominal dust concentration. *J Loss Prevent Process Ind*. 2014;27:8–12.
31. Tong ZB, Zheng B, Yang RY, Yu AB, Chan HK. CFD-DEM investigation of the dispersion mechanisms in commercial dry powder inhalers. *Powder Technol*. 2013;240:19–24.
32. Breault RW. A review of gas–solid dispersion and mass transfer coefficient correlations in circulating fluidized beds. *Powder Technol*. 2006;163:9–17.
33. Jiradilok V, Gidaspow D, Breault RW, Shadle LJ, Guenther C, Shi S. Computation of turbulence and dispersion of cork in the NETL riser. *Chem Eng Sci*. 2008;63:2135–2148.
34. Zhang Y, Zhong W, Jin B, Xiao R. Investigating the particle dispersion in a spout-fluid bed using particle trajectory. *Int J Chem React Eng*. 2012;10:A80.
35. Harris AT, Davidson JF, Thorpe RB. Particle residence time distributions in circulating fluidised beds. *Chem Eng Sci*. 2003;58:2181–2202.
36. Zhong W, Zhang Y, Jin B. Novel method to study the particle circulation in a flat-bottom spout-fluid bed. *Energy Fuels*. 2010;24:5131–5138.
37. Yang S, Luo K, Fang M, Zhang K, Fan J. Parallel CFD–DEM modeling of the hydrodynamics in a lab-scale double slot-rectangular spouted bed with a partition plate. *Chem Eng J*. 2014;236:158–170.
38. Gidaspow D. Multiphase Flow and Fluidization: Continuum and Kinetic Theory Descriptions, 1st ed. San Diego: Academic Press, 1994.
39. Yang RY, Zou RP, Yu AB. Numerical study of the packing of wet coarse uniform spheres. *AIChE J*. 2003;49:1656–1666.
40. Cundall PA, Strack ODL. A discrete numerical model for granular assemblies. *Geotechnique*. 1979;9:47–65.
41. Farzaneh M, Sasic S, Almstedt A, Johnsson F, Pallarès D. A study of fuel particle movement in fluidized beds. *Ind Eng Chem Res*. 2013;52:5791–5805.
42. Niklasson F, Thunman H, Johnsson F, Leckner B. Estimation of solids mixing in a fluidized-bed combustor. *Ind Eng Chem Res*. 2002;41:4663–4673.
43. Zhu HP, Zhou ZY, Yang RY, Yu AB. Discrete particle simulation of particulate systems: theoretical developments. *Chem Eng Sci*. 2007;62:3378–3396.
44. Issa RI. Solution of the implicitly discretised fluid flow equations by operator-splitting. *J Comput Phys*. 1986;62:40–65.
45. Li Y, Xu Y, Thornton C. A comparison of discrete element simulations and experiments for 'sandpiles' composed of spherical particles. *Powder Technol*. 2005;160:219–228.
46. Raji AO, Favier JF. Model for the deformation in agricultural and food particulate materials under bulk compressive loading using

discrete element method. I: theory, model development and validation. *J Food Eng*. 2004;64:359–371.
47. Kuo HP, Knight PC, Parker DJ, Tsuji Y, Adams MJ, Seville JPK. The influence of DEM simulation parameters on the particle behaviour in a V-mixer. *Chem Eng Sci*. 2002;57:3621–3638.
48. Du W, Bao X, Xu J, Wei W. Computational fluid dynamics (CFD) modeling of spouted bed: influence of frictional stress, maximum packing limit and coefficient of restitution of particles. *Chem Eng Sci*. 2006;61:4558–4570.
49. Lan X, Xu C, Gao J, Al-Dahhan M. Influence of solid-phase wall boundary condition on CFD simulation of spouted beds. *Chem Eng Sci*. 2012;69:419–430.

Manuscript received Jan. 21, 2014, and revision received Mar. 31, 2014.